Journal of Solid State Chemistry **142,** 214–219 (1999)
Article ID jssc.1998.8037, available online at http://www.idealibrary.com on IDEAL®

Crystal Structure and Vibrational Spectra of Li_2BAlO_4

V. Psycharis,*,[1] I. A. Kapoutsis,† and G. D. Chryssikos†

*Institute of Materials Science, NCSR "Demokritos," 15310 Ag. Paraskevi, Attiki, Greece; and †Theoretical and Physical Chemistry Institute, National Hellenic Research Foundation, 48 Vass. Constantinou Avenue, Athens 11635, Greece

Received April 21, 1998; in revised form September 14, 1998; accepted September 17, 1998

The structure of Li_2BAlO_4 is solved *ab initio* by a powder X-ray diffraction technique. The unit cell of this metaboroaluminate compound is monoclinic (space group $P2_1/c$, $a=6.2720(3)$ Å, $b=5.0701(3)$ Å, $c=10.2989(6)$ Å, $\beta=95.882(2)^\circ$, $Z=4$, $\rho_{calc}=2.36$ g/cm^3). Its network consists of infinite chains of metaaluminate tetrahedra, which are cross-linked by metaborate triangles in a way that leads to the formation of $B_2Al_2O_8^{4-}$ rings. These anionic groups are charge-balanced by two crystallographically distinct pairs of four-coordinated lithium ions. The infrared and Raman spectra $Li_2{}^{n}BAlO_4$ and $Li_2{}^{10}BAlO_4$ are reported, and the assignments of their main features are discussed in light of the spectra of relevant compounds. Vibrational spectroscopic tools for the identification of mixed metaboroaluminate network sequences are proposed.

Key Words: **Li_2BAlO_4; meta-boroaluminate crystals; ab initio powder X-ray diffraction; infrared; Raman**

1. INTRODUCTION

A lithium metaborate–metaaluminate compound with a 1:1 boron to aluminum ratio, Li_2BAlO_4, has been reported by Kim and Hummel (1) but its structure has remained unknown. Three alkaline earth compounds with the same network stoichiometry are known: $CaBAlO_4$ and $SrBAlO_4$ consist of metaaluminate tetrahedra, $Al\emptyset_4^-$, and metaborate triangles, $B\emptyset_2O^-$ (Ø, oxygen atom bridging two boron centers; O, nonbridging oxygen). These units form condensed $BAl_2O_6^{3-}$ rings which share one aluminate tetrahedron (2, 3). Instead, $MgBAlO_4$ has a spinel structure with aluminum assuming an octahedral coordination to oxygen (4).

Since then, a second mixed network compound along the $LiBO_2$–$LiAlO_2$ join, $Li_3B_2AlO_6$, has been synthesized and evaluated crystallographically by Abdullaev and Mamedov (5). The network of $Li_3B_2AlO_6$ was found to consist of $B_2Al_2O_8^{4-}$ rings made of alternating $Al\emptyset_4^-$ and $B\emptyset_2O^-$ units and linked via $B\emptyset_2O^-$ "spacers" (5).

In the course of a recent investigation of glasses and crystals along the $LiBO_2$–$LiAlO_2$ join, Li_2BAlO_4 has been obtained in polycrystalline form (6). Every $B\emptyset_2O^-$ triangle is linked to two $Al\emptyset_4^-$ species, and there is some indication for the presence of Al–O–Al bridges. Preliminary vibrational spectroscopic comparisons (6) have indicated that Li_2BAlO_4 is structurally different than $CaBAlO_4$ or $SrBAlO_4$ and instead exhibits similarities to $Li_3B_2AlO_6$.

In this paper we report on the structural determination of Li_2BAlO_4 by a powder X-ray diffraction technique. We also report the infrared and Raman spectra of ^{10}B-enriched Li_2BAlO_4 and advance the analysis of the vibrational data in light of the newly determined crystal structure.

2. EXPERIMENTAL

a. Chemical Preparation

Finely ground and dry Li_2CO_3, B_2O_3, and Al_2O_3 (corundum), mixed in stoichiometric proportions have been pelletized and used as starting materials. For the isotopically enriched sample, $H_3{}^{10}BO_3$ (97 at.% ^{10}B, Aldrich) was employed instead of $^{n}B_2O_3$. Polycrystalline Li_2BAlO_4 samples were prepared by solid-state reaction at 600°C for ca. 2 months. The progress of the reaction was monitored by Raman spectroscopy. The final product contained ca. 3% γ-$LiAlO_2$, determined by X-ray diffraction. More details on the synthesis of Li_2BAlO_4 can be found in Ref. (6).

b. X-ray Diffraction

X-ray powder diffraction data were collected with a D500 SIEMENS diffractometer employing Cu$K\alpha$ radiation and a secondary beam graphite monochromator. The measured 2θ range (20–110°) was scanned in steps of 0.03° with a counting time of 6 s/step. The aperture and the soller slits were set at 1.0°.

[1]To whom correspondence should be addressed. Fax: 301 6519430. E-mail: vpsychar@ims.ariadne-t.gr.

0022-4596/99 $30.00

c. Vibrational Spectroscopy

Infrared spectra were collected from the smooth surface of the pelletized sample on a Fourier transform spectrometer (Bruker 113v) operating in the 11° specular reflectance mode. An appropriate selection of sources, beamsplitters and detectors ensured continuous data acquisition over the 300–4000 cm^{-1} range. The spectra are the average of 200 scans at 2 cm^{-1} resolution. The reflectance data have been transformed by Kramers–Kronig analysis and presented in the absorption coefficient formalism.

Raman spectra have been obtained on a double monochromator spectrometer (Jobin-Yvon HG2S) at 90° scattering geometry and ca. 5 cm^{-1} spectral resolution. The 488.0 blue line (500 mW) of an argon-ion laser (Spectra Physics 165) was used for excitation.

3. RESULTS AND DISCUSSION

a. Crystal Data and Structure Determination

The final crystal data for Li_2BAlO_4 are given in Table 2. The unit cell was calculated using the Visser program (7) and found to be monoclinic with approximate dimensions: $a = 6.268$ Å, $b = 5.069$ Å, $c = 10.295$ Å, $\beta = 95.89°$. On the basis of these dimensions a list of all possible reflections can be derived and compared to the reflections observed in the XRD spectrum of the sample. This comparison reveals the systematic absence of the conditions $h\ 0\ l$ with $l = 2n + 1$ and $0\ k\ l$ with $k = 2n + 1$. Thus, the unit cell belongs to the space group $P2_1/c$. Subsequently, the structure was solved by using the procedure described in (8).

Approximate values for the observed structure factors were obtained using the Fullprof program (9) in the Full Pattern Decomposition mode. The above approximate values for the unit cell and the space group were used to input the program. The intensity distribution was described by the Pearson VII function. The unit cell parameters, the background parameters, the exponent of the Pearson VII function and the full width parameters were refined. The final values for the unit cell dimensions were $a = 6.2683(2)$ Å, $b = 5.0673(2)$ Å, $c = 10.2899(3)$ Å, and $\beta = 95.88(1)°$. The agreement indices (R factors (10)) converged to the values $R_p = 15.0$, $R_{wp} = 22.8$, $R_B = 2.47$, and $R_{exp} = 3.53\%$.

The number of independent reflections in the refined 2θ range, was 417. The application of Patterson synthesis by using the SHELXS-86 program (10a) was not successful in locating any atom. By applying the direct methods an atom was located at the site No. 1 of Table 1 and was tentatively identified as A1. Difference Fourier synthesis (SHELXL-93 (10b)) and the use of the |Fobs| values derived by the Full Pattern Decomposition method, located three more atoms (Nos. 2–4, Table 1), which were considered as oxygens. All attempts to locate more atoms by these techniques were unsuccessful. More accurate |Fobs| values were obtained by applying the Rietveld intensity decomposition formula (11) to the starting model of Al, O(1), O(2), O(3) at positions listed in Table 1.

Rietveld refinement lead to the optimization of the unit cell dimensions and the background parameters (11, 12). The profile shape parameters (Pearson VII exponent) and the full width parameters were kept constant at the values derived from the Full Pattern Decomposition run. These new |Fobs| values were used to input difference Fourier synthesis with the program SHELXL-93 (10b) and yielded the locations of two more atoms (Nos. 5 and 6 of Table 1). These were assigned to oxygen and boron, respectively. A second iteration of Rietveld refinement based on atoms Al, O(1), O(2), O(3), O(4), and B produced new and more accurate |Fobs| values. Based on these values, it became possible to locate the sites of Li(1) and Li(2) atoms (Nos. 7 and 8, Table 1) by difference Fourier synthesis. The final values of the atom positions and the temperature factors were obtained by the standard Rietveld refinement method (12) and they are listed in Table 2. The temperature factors

TABLE 1
Atom Sites Found by Direct Methods and Difference Fourier Synthesis

Site No.	x	y	z	Assignment
1	0.463	0.638	0.63	Al
2	0.62	0.857	0.775	O(1)
3	0.02	0.835	0.358	O(2)
4	0.66	0.3478	0.987	O(3)
5	0.24	0.152	0.875	O(4)
6	0.80	0.329	0.557	B
7	0.22	0.349	0.098	Li(1)
8	0.1	0.365	0.781	Li(2)

TABLE 2
Crystallographic Data for Li_2AlBO_4

Atom	Site	x	y	z	B (Å^2)
Al	4*e*	0.4993(4)	0.6448(5)	0.6581(2)	0.85(4)
B	4*e*	0.805(1)	0.314(2)	0.559(1)	1.7(2)
Li(1)	4*e*	0.221(2)	0.334(3)	0.072(1)	1.9(2)
Li(2)	4*e*	0.081(2)	0.360(3)	0.788(1)	1.9(2)
O(1)	4*e*	0.6008(6)	0.8519(9)	0.7846(5)	0.86(5)
O(2)	4*e*	0.0487(7)	0.7997(8)	0.3577(5)	0.86(5)
O(3)	4*e*	0.7030(7)	0.3050(8)	0.9504(5)	0.85(5)
O(4)	4*e*	0.2608(6)	0.0867(8)	0.9237(4)	0.85(5)

Note. Space group No. 14 $P2_1/c$, unique axis b. unit cell dimensions: $a = 6.2720(3)$ Å, $b = 5.0701(3)$ Å, $c = 10.2989(6)$ Å, $\beta = 95.882(2)°$, $V = 325.78$ Å^3, $Z = 4$, and $\rho_{calc} = 2.63$ g/cm^3. Agreement indices (R-factors): $R_p = 6.17$, $R_{wp} = 11.13$, $R_B = 5.14$, $R_{exp} = 2.75\%$.

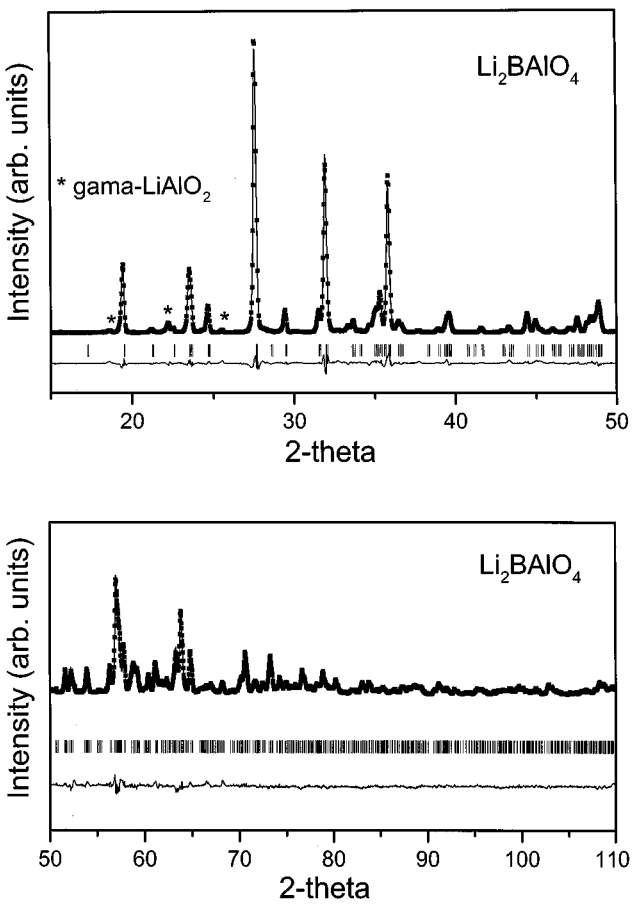

FIG. 1. XRD spectrum of Li_2BAlO_4 refined by the Rietveld method. The continuous line corresponds to the calculated spectrum, vertical bars (|) indicate the position of Bragg peaks. The bottom trace depicts the difference between the experimental and the calculated intensity values. For clarity, the spectrum is presented in two separate 2θ regions.

were refined independently for each atomic species (a common temperature factor was used for Li and O atoms). Traces of the tetragonal γ-$LiAlO_2$ (17) phase are detected and found by Rietveld analysis to be less than 3%. The Rietveld refinement diagrams are presented in Fig. 1.

b. Description of the Structure

The unit cell of Li_2BAlO_4 is shown in Fig. 2. The crystal structure (shown in Fig. 3) can be described as consisting of aluminoborate sheets spread parallel to the *b–c* plane and held together by lithium ions. Each sheet consists of chains of corner sharing $AlØ_4^-$ tetrahedra related by the screw axis running along the direction of the *b*-axis. Adjacent chains are cross-linked by pairs of centrosymmetrically related $BØ_2O^-$ triangles (Fig. 3a). As a result of this cross-linking, metaboroaluminate rings, $B_2Al_2O_8^{4-}$, are formed of alternating corner-sharing $AlØ_4^-$ tetrahedra and $BØ_2O^-$ triangles. Opposite ring polyhedra of the same kind assume a chair conformation. Looking down the *c*-axis, the sheets appear to consist of an aluminate "core" monolayer, with both surfaces decorated by metaborate triangles. The thickness of each sheet, including the charge balancing Li^+ ions, equals the length of the *a*-axis, 6.271(3) Å (Fig. 3b). The main interatomic bond distances and angles are included in Table 3.

To provide a check on the consistency of the crystal solution, the bond valences or strengths, *s*, have been calculated according to the Brown and Altermatt parameters (13) and are reported in Table 4. It can be seen that the bond valence sum of each atom of the unit cell is in fairly good agreement with the formal oxidation state.

Of the three oxygen atoms in the coordination sphere of B, O(2) has a terminal character, manifested by the short $B–O^-$ distance and, consequently, by a bond strength higher than unity. On the contrary, the remaining B–O(3) and B–O(4) are longer (1.37 and 1.46 Å, respectively). For comparison, the bond lengths (strengths) in α-$LiBO_2$ are $B–O^- = 1.323$ Å ($s = 1.14$), as well as $B–Ø = 1.392$ Å ($s = 0.90$), and 1.410 Å ($s = 0.94$), leading to an average length of 1.375 Å and a boron valence $\Sigma s = 2.98$ (15). This comparison demonstrates that the boron site of Li_2BAlO_4 is characterized by a very pronounced removal of the degeneracy of the two bridging oxygens. The O(2)–B–O(3) moiety is strongly interconnected in a way reminiscent of gaseous $LiBO_2$ (15) and interacts weakly to O(4), establishing a bond which is typical of tetrahedral rather than trigonal borate arrangements (16).

The aluminate tetrahedra are distorted, with two bonds at ca. 1.74 Å and the remaining two at ca. 1.8 Å. The average Al–O bond length (1.775 Å) is intermediate compared to those found in γ-$LiAlO_2$ (1.761 Å, Ref. (17)) and $Li_3B_2AlO_6$ (1.888 Å, Ref. (5)). More notably, the O(1)′–O(4) edge length, as well as the corresponding O(1)′–Al–O(4) angle, both take very low values (2.747 Å and 100.8°). A similar distortion is observed in γ-$LiAlO_2$, where the corresponding edge length and angle take the values 2.737 Å and 101.6° (17). In both structures, the O(1)′–O(4) edge is shared with a Li tetrahedron (dotted line in Fig. 2).

Of the two distinct Li tetrahedra, Li(1) has relatively uniform Li–O bond lengths, but Li(2) is heavily distorted, with two bonds (Li(2)–O(1) and Li(2)–O(4)) accounting each for less than 15% of the overall bond valence (Table 4). Li(1) links three bridging oxygen atoms of one metaboroaluminate sheet, with the nonbridging oxygen on the boron of the next sheet, and does not share edges with any borate or aluminate polyhedron. On the contrary, Li(2) shares edges with one aluminate tetrahedron (see above) and links it to two nonbridging oxygens of the same and next sheets (Fig. 3b). As a result of edge-sharing with the Al tetrahedron, the O(1)–Li(2)–O(4) angle is only 77.3° (cf. 83.29° for γ-$LiAlO_2$, Ref. 17). The two lithium tetrahedra also share a common

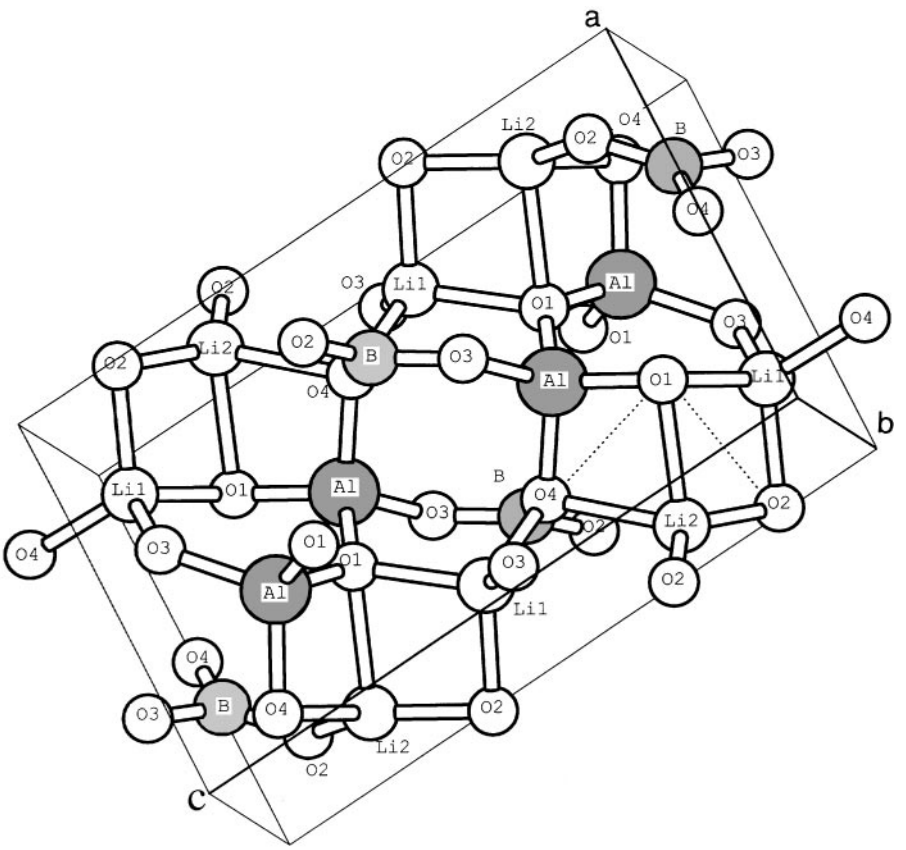

FIG. 2. The unit cell of Li_2BAlO_4. Dotted lines indicate common edges of the Li(2) tetrahedron with the Al and Li(1) tetrahedra. For details see text.

edge, which takes a low value (O(1)–O(2′) = 2.935 Å, O(1)–Li(1)–O(2) = 93.2°). A similar sharing occurs in α-$LiBO_2$, leading to an edge length of 2.985 Å and an angle of 96.04° (14).

All the oxygen atoms are bridging two boron or aluminium network centers, with the exception of O(2), which is nonbridging. If the Li ions are considered as well, O(1), O(2), and O(4) become four-coordinated to the cationic centers, while O(3) remains trigonal (Table 4).

c. *Vibrational Spectra*

The infrared absorption and Raman scattering spectra of $Li_2{}^nBAlO_4$ and $Li_2{}^{10}BAlO_4$ are shown in Figs. 4 and 5, respectively. Following detailed assignments discussed in an earlier publication (6), we attribute the bands active above 1000 cm^{-1} in both the infrared and Raman spectra to the stretching vibrations of metaborate triangles. These bands exhibit a large frequency dependence on boron isotope mass. The boron oxygen stretching modes appear to be split in both the infrared (centered at ca. 1220- and ca. 1420 cm^{-1} for $Li_2{}^nBAIO_4$) and the Raman spectra (1153- and 1362 cm^{-1}) and thus confirm the asymmetric bonding of the metaborate triangles. Of particular interest is the position of the highest frequency Raman band (1362 cm^{-1}). This band is mainly due to the B–O^- stretching mode (18). The corresponding feature in the spectrum of α-Li^nBO_2 is centered at ca. 1480 cm^{-1} (18, 19). In metaborate compounds like $Ba_2LiB_5O_{10}$, where every metaborate triangle is bonded to two metaborate tetrahedra, the B–O^- stretch appears to be shifted to lower frequencies (ca. 1400 cm^{-1}). This frequency decrease is related to the elongation of this bond as a result of enhanced π interactions between the empty p_z orbital on the boron and the basic oxygens of its tetrahedral metaborate neighbors (18). In Li_2BAlO_4 the shift is even more pronounced due to the higher basicity of the metaaluminate tetrahedra and can be used as a spectroscopic indicator for the presence of mixed metaboroaluminate networks (6).

Strong features in the 900–1000 cm^{-1} range (957 cm^{-1} and 907 and 956 cm^{-1}, in the Raman and infrared spectra of $Li_2{}^nBAlO_4$, respectively), show negligible or no dependence on B mass and are attributed to the stretching vibrations of metaaluminate tetrahedra. The strong Raman band at 485 cm^{-1} is also due to stretching–bending vibrations of $AlØ_4^-$ units. A detailed discussion on the aluminate modes in $Li_2{}^nBAlO_4$ and related crystals can be found in Ref. 6. A set of well-defined, medium-intensity bands between 700 and 800 cm^{-1} in the infrared and Raman spectra are in the

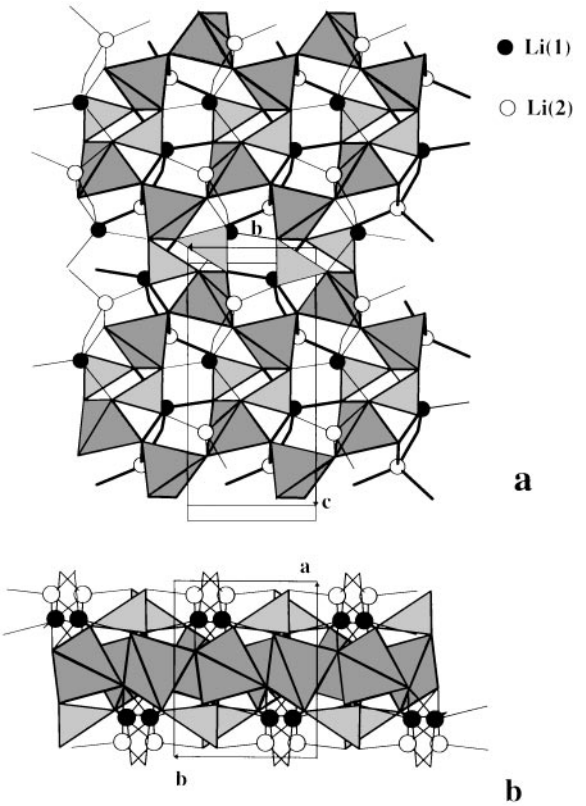

FIG. 3. (a) The metaboroaluminate sheet of Li_2BAlO_4 viewed down the *a*-axis. Chains of aluminate tetrahedra (dark shading) are cross-linked by metaborate triangles (light shading). Heavy and thin lines depict lithium–oxygen bonds below and above the sheet, respectively. (b) The same sheet viewed down the *c*-axis.

TABLE 3
Bond Lengths (Å), Angles (Degrees), and Selected Interatomic Distances (Å), in Li_2AlBO_4

Bond lengths (Å)		Angles (degrees)		Selected interatomic distances (Å)	
Al–O(1)	1.742(5)	O(1)-Al-O(3)	109.9(2)	O(1)–O(1)′	2.889(6)
Al–O(1)′	1.739(5)	O(1)-Al-O(4)	111.3(2)	O(1)–O(3)	2.895(6)
Al–O(3)	1.797(5)	O(1)′–Al-O(1)	112.2(2)	O(1)–O(4)	2.940(6)
Al–O(4)	1.822(4)	O(1)′–Al-O(3)	111.9(2)	O(1)′–O(3)	2.933(6)
		O(1)′–Al-O(4)	100.8(2)	O(1)′–O(4)	2.747(6)
		O(3)-Al-O(4)	110.5(2)	O(3)–O(4)	2.972(6)
Av. value	1.775(21)				2.896(32)
B–O(2)	1.322(9)	O(2)–B–O(3)	124.9(6)	O(2)–O(3)	2.387(6)
B–O(3)	1.37(1)	O(2)–B–O(4)	121.3(6)	O(2)–O(4)	2.426(6)
B–O(4)	1.46(1)	O(3)–B–O(4)	113.7(5)	O(3)–O(4)	2.369(6)
Av. value	1.384(40)				2.394(17)
Li(1)–O(1)	2.00(1)	O(1)-Li(1)-O(2)	97.3(5)	O(1)–O(2)	2.935(6)
Li(1)–O(2)	1.91(1)	O(1)-Li(1)-O(3)	114.5(5)	O(1)–O(3)	3.285(6)
Li(1)–O(3)	1.91(2)	O(1)-Li(1)-O(4)	99.4(5)	O(1)–O(4)	3.056(6)
Li(1)–O(4)	2.01(1)	O(2)-Li(1)-O(3)	111.9(6)	O(2)–O(3)	3.171(6)
		O(2)-Li(1)-O(4)	114.4(5)	O(2)–O(4)	3.301(6)
		O(3)-Li(1)-O(4)	117.0(5)	O(3)–O(4)	3.344(6)
Av. value	1.958(28)				3.182(65)
Li(2)–O(1)	2.20(1)	O(1)-Li(2)-O(2)	106.4(5)	O(1)–O(2)	3.280(6)
Li(2)–O(2)	1.82(1)	O(1)-Li(2)-O(2)′	93.2(5)	O(1)–O(2)′	2.935(6)
Li(2)–O(2)′	1.89(2)	O(1)-Li(2)-O(4)	77.3(6)	O(1)–O(4)	2.747(6)
Li(2)–O(4)	2.19(1)	O(2)-Li(2)-O(4)	113.8(4)	O(2)–O(2)′	3.383(6)
		O(2)′–Li(2)-O(2)	131.5(6)	O(2)–O(4)	3.424(6)
		O(2)′–Li(2)-O(4)	113.6(6)	O(2)′–O(4)	3.368(6)
Av. value	2.025(99)				3.19(11)

frequency range where the out-of-plane bending modes of the $B\emptyset_2O^-$ units are expected (see for example Ref. (19) for the spectra of α-$LiBO_2$). Finally, bands below ca. 400 cm^{-1} involve motions of Li^+ ions and thus exhibit little or no dependence on boron isotope ratio.

4. CONCLUSIONS

In the present work we report the *ab initio* solution of the Li_2BAlO_4 crystal structure by means of a powder X-ray diffraction technique. We aim, therefore, to broaden our understanding for those compounds that are difficult to grow in single crystal forms. By the same token, we hope to open new possibilities for the convenient study of low temperature devitrification products, which are relevant to the structure of glasses, but cannot be grown from the melt and studied by conventional techniques (20).

Li_2BAlO_4 crystallizes in a hitherto unknown structure and exhibits a network made of $Al\emptyset_4^-$ tetrahedra and $B\emptyset_2O^-$ triangles. The same polyhedra are found in the networks of the high-temperature lithium metaaluminate (γ-$LiAlO_2$, Ref. (17)) and metaborate (α-$LiBO_2$, Ref. (14)) polymorphs, to which Li_2BAlO_4 dissociates sluggishly above ca. 750°C. The similarities between Li_2BAlO_4 on one hand, and $CaBAlO_4$ or $SrBAlO_4$ on the other, are limited to the type of the primary building blocks of their covalent networks (2, 3). In these latter crystals, the $B\emptyset_2O^-$ units do not cross-link adjacent metaaluminate chains as in Li_2BAlO_4. Instead, they bridge adjacent $Al\emptyset_4^-$ tetrahedra of the same chain, assuming positions similar to those occupied by Li(1) in Li_2AlBO_4. As a result, the

TABLE 4
B–O, Al–O, and Li–O Bond Valences in Li_2BAlO_4

	O(1)	O(2)	O(3)	O(4)	∑s
B		1.15	1.03	0.77	2.95
Al	0.79, 0.80		0.68	0.64	2.91
Li(1)	0.25	0.30	0.29	0.23	1.07
Li(2)	0.14	0.37, 0.32		0.14	0.97
∑s	1.97	2.14	2.00	1.78	

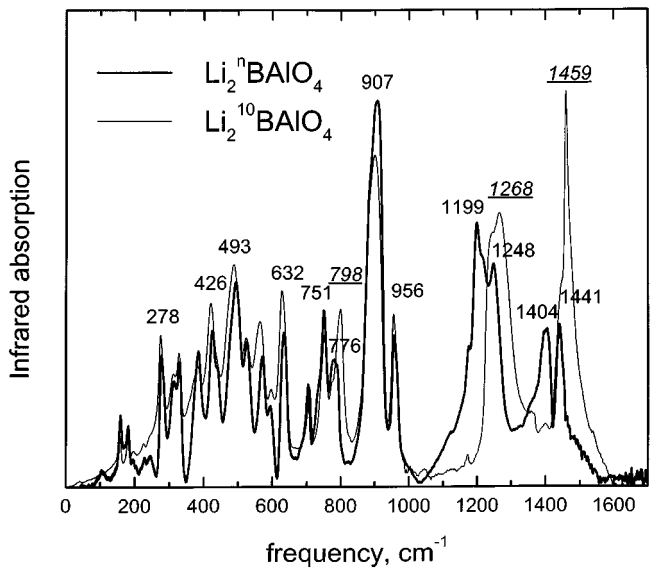

FIG. 4. Infrared absorption spectra of $Li_2{}^nBAlO_4$ (thick line) and $Li_2{}^{10}BAlO_4$ (thin line). Underlined legends correspond to characteristic peak maxima of the ^{10}B-enriched sample.

metaboroaluminate subnetwork is two-dimensional in Li_2BAlO_4 and pseudo-one-dimensional (tube-like) in $CaBAlO_4$ or $SrBAlO_4$.

Li_2BAlO_4 exhibits structural similarities to $Li_3B_2AlO_6$ (and its isostructural $Li_3B_2GaO_6$), the networks of which were also found to contain the same eight-membered $B_2Al_2O_8^{4-}$ (or $B_2Ga_2O_8^{4-}$) rings (5, 21). In terms of intermediate range order, another similarity can be found between Li_2BAlO_4 and γ-$LiAlO_2$ (17). It involves the occurrence in both structures of edge-sharing between the Al and Li(2) tetrahedra, which results in unusually low values for the O(1)′–O(4) distance and the corresponding O(1)′–Al–O(4) and O(1)′–Li(2)–O(4) angles. Edge-sharing is also observed between the Li(1) and the Li(2) tetrahedra as in α-$LiBO_2$ (14).

Despite these structural similarities, it has not become obvious how equimolar quantities of γ-$LiAlO_2$ and α-$LiBO_2$ combine at (or below) 750°C to form Li_2BAlO_4. Hence, the long-range structural interconversions in the lithium metaboroaluminate phase diagram (1) remain the subject of ongoing research.

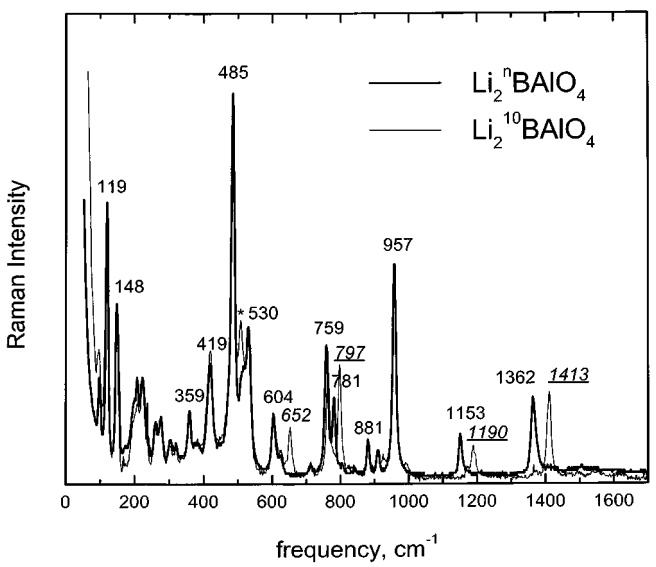

FIG. 5. Raman spectra of $Li_2{}^nBAlO_4$ (thick line) and $Li_2{}^{10}BAlO_4$ (thin line). Underlined legends correspond to characteristic peak maxima of the ^{10}B-enriched sample. The asterisk marks a peak due to traces of γ-$LiAlO_2$.

ACKNOWLEDGMENTS

Dr. V. Perdikatsis is thanked for his assistance in plotting the crystal structure using Atoms by Shape software. This work was financially supported by NCSR "Demokritos" and NHRF.

REFERENCES

1. K. H. Kim and F. A. Hummel, *J. Am. Ceram. Soc.* **45,** 487 (1962).
2. W. Schuckman, *Neues Jahrb. Mineral. Monatsh.* **3/4,** 80 (1968).
3. T. Nagai and M. Ihara, *Yogyo-Kyokai-Shi* **80,** 14 (1972).
4. M. P. O'Horo, A. L. Frisillo, and W. B. White, *J. Phys. Chem. Solids* **34,** 23 (1973).
5. G. K. Abdullaev and K. S. Mamedov, *Sov. Phys. Crystallogr.* **27,** 229 (1982).
6. G. D. Chryssikos, M. S. Bitsis, J. A. Kapoutsis, and E. I. Kamitsos, *J. Non-Cryst. Solids* **217,** 278 (1997).
7. J. W. Visser, *Acta Crystallogr.* **2,** 89 (1969).
8. V. Psycharis, O. Kalogirou, D. Niarchos, and M. Gjioka, *J. Alloys Compounds* **234,** 62 (1996).
9. J. Rodriquez-Carvajal, M. T. Fernadez-Diaz, and J. L. Martinez, *J. Phys. Condens. Matter* **3,** 3215, (1991).
10. (a) Sheldrick, G. M., "SHELXS-86." University of Goettingen, Germany, 1986. (b) Sheldrick, G. M., "SHELXL 93: Crystal Structure Refinement". Univ. of Goettingen, Germany, 1993.
11. H. M. Rietveld, *J. Appl. Crystallogr.* **2,** 65 (1969).
12. D. A. Wiles and R. A. Young, *J. Appl. Crystallogr.* **14,** 149 (1981).
13. I. D. Brown and D. Altermatt, *Acta Crystallogr.* **B41,** 244 (1985).
14. A. Kirfel, G. Will, and R. F. Stewart, *Acta Crystallogr.* **B39,** 175 (1983).
15. Minh Tho Nguyen, *J. Mol. Sci.* (Theochem) **136,** 371 (1986).
16. G. D. Chryssikos, J. A. Kapoutsis, A. P. Patsis, and E. I. Kamitsos, *Spectrochim. Acta* **47A,** 1117 (1991).
17. M. Marezio, *Acta Crystallogr.* **19,** 396 (1965).
18. G. D. Chryssikos, *J. Raman Spectrosc.* **22,** 645 (1991).
19. A. Rulmont and M. Almou, *Spectrochim. Acta* **45A,** 603 (1989).
20. G. D. Chryssikos and E. I. Kamitsos, "Proceedings of the 2nd International Conference of Borate Glasses, Crystals and Melts" (A. C. Wright and S. A. Feller, Eds.), pp. 303–312. Soc. Glass Technology, 1997.
21. G. K. Abdullaev and K. S. Mamedov, *Proc. Acad. Sci. USSR, Inorganic Mater.* **73,** 881 (1972).